

Study of human forearm posture maintenance with a physiologically based robotic arm and spinal level neural controller

Ching-Ping Chou, Blake Hannaford

Department of Electrical Engineering, University of Washington, Seattle, WA 98195-2500, USA

Received: 22 April 1996 / Accepted in revised form: 6 November 1996

Abstract. The goals of this research are: (1) to apply knowledge of human neuro-musculo-skeletal motion control to a biomechanically designed, neural controlled, ‘anthroform’ robotic arm system, (2) to demonstrate that such a system is capable of responses that match those of the human arm reasonably well in comparable experiments, and (3) to utilize the anthroform arm system to study some controversial issues and to predict new phenomena of the human motion control system. A physiologically analogous artificial neural network controller and an anatomically accurate robotic testing elbow are applied in this study. In order to build the physical elbow system to have mechanical properties as close as possible to the human arm, McKibben pneumatic artificial muscles, force sensors, and mechanical muscle spindles are integrated in the system with anatomically accurate muscle attachment points. A physiologically analogous, artificial neural network controller is used to emulate the behavior of spinal segmental reflex circuitry including Ia and Ib afferent feedbacks. Systematic experiments of elbow posture maintenance are performed and compared with physiological experimental data. New experiments are performed in which responses to torque perturbation are measured when selected afferent pathways are blocked. A ‘covariance diagram’ is introduced. And a linear model is used to help to analyze the roles of system components. The results show that muscle co-contraction and Ia afference with gamma dynamic motoneuron excitation are two efficient ways to increase joint stiffness and damping, which in turn reduces the mechanical sensitivity of the joint to external perturbation and shortens the settling time of the system.

1 Introduction

While modern control research is still developing a number of theories to solve motion control problems, the

human musculo-skeletal motion system has been proven to succeed by nature for thousands of years. Scientists have long attempted to understand the human motion control method. However, the complexity of the system and the lack of technology made this very difficult. With the development of advanced electronic instruments and medical techniques, ever more insight into the human nervous system has been gained, and increasing numbers researchers have entered this area.

The approach to human motion control research can be either top-down or bottom-up. While the top-down approach starts from the conceptual layer (task) and proceeds through the functional layer (block) to the physical (device) layer, the bottom-up approach reverses this ordering. The foci can be roughly partitioned into high-level control and low-level control. High-level control focuses on brain functionalities, such as motion planning, coordination, and learning (Raibert 1978; Loeb 1987; Gomi and Kawato 1993). Low-level control focuses on spinal cord functionalities, such as the short latency reflex and the integration of voluntary command into spinal neural circuitries. Since this research area is still developing, neither the top-down nor the bottom-up approach has achieved full understanding of the system. As a result, it is very reasonable that high-level control research chooses a top-down approach and low-level control research chooses a bottom-up approach.

The goals of this research are: (1) to apply knowledge of human neuro-musculo-skeletal motion control to a biomechanically designed, neural controlled, ‘anthroform’ robotic arm system, (2) to demonstrate that such a system is capable of responses that match those of the human arm reasonably well in comparable experiments, and (3) to utilize the anthroform arm system to study some controversial issues and to predict new phenomena of the human motion control system.

We start by focusing on low-level control and using a bottom-up approach. Existing low-level neural control research can be partitioned into two stages: the controller and the plant. The controller can be further classified into three types: (1) a conventional feedback controller with minimal or very abstract neural control concepts

(Ramos et al. 1990), (2) an artificial neural network controller with functional reproduction of human neural circuitry (Bullock et al. 1992; Hannaford et al. 1995), and (3) a combination of the above (Lan and Crago 1994). Similarly, the plant can be classified into three types: (1) mathematical dynamics models (Ramos et al. 1990; Bullock et al. 1992; Lan and Crago 1994), (2) conventional robotic arms (Inoue 1988), and (3) anthropomorphic robotic arms (Hannaford et al. 1995). Here we define the term 'anthroform' to describe a robotic arm in which all aspects of its design are specified in terms of emulation of the corresponding functions of the human arm. Many of these approaches have established new research directions.

1.1 Actuators

One of the most fundamental elements in our project is the actuator which will substitute for skeletal muscles in the system. We cannot expect a technologically realized actuator to simulate accurately all the static and dynamic behaviors of muscle. However, we would like the ideal actuator technology for this application to meet the following requirements (no particular order):

- Strength to weight ratio (N kg^{-1}) and tension intensity (N cm^{-2}) equal to or exceeding those of skeletal muscle.
- Contraction ratio ($\Delta L/L$) and speed of contraction [$(\Delta L/L_0)t^{-1}$] comparable to those of skeletal muscle.
- Variation of force with length comparable to that described in muscle (Gordon et al. 1966).
- Damping behavior comparable to skeletal muscle – for example, a nonlinear damping following Hill's (1938) model – would be an excellent approximation. Although there are many known subtleties to the dynamics of muscle contraction, accurate reproduction of Hill's force-velocity relation would represent a huge advance towards more biological actuation characteristics.
- Flexibility to curve around bones and ligaments and to rub against neighboring actuators (for example in the deltoid muscle) so that it can be integrated within the skeleton.
- Ability to be easily manufactured in a range of physiologically relevant lengths at low cost.
- Compatibility with widely available power sources and environmental conditions.
- Reliability to perform many cycles without failure. This will be especially valuable for future experiments in motor learning control.

No actuator available today meets all these criteria. In earlier studies, we tested McKibben pneumatic artificial muscle actuators in a static and dynamic testing machine, and reviewed their properties in comparison with human muscle (Chou and Hannaford 1994, 1996; Chou 1996). This testing, along with kinematic, dynamic, and thermodynamic analysis, showed that McKibben actuators satisfy or exceed six of the eight criteria. For example, the tension intensity of the actuators we are using (116 N cm^{-2}) and the strength to weight ratio

($>3900 \text{ N kg}^{-1}$) far exceed those of skeletal muscle. However, our testing revealed that McKibben actuators lack the desired damping characteristics of muscle and specifically lack nonlinear Hill-type damping. Although this unrealistic feature of the actuators will affect the results, their excellent performance on the other six criteria led us to select them for the arm implementation (Hannaford and Winters 1990; Hannaford et al. 1995). Work now under way in our laboratory is aimed at an improved McKibben actuator with intrinsic Hill-type damping.

1.2 Testing elbow

Implementation of reflex-like control on the arm requires sensory inputs for kinesthetic information. Testing requires precise, nonphysiological measurements of limb position, as well as the ability to apply controlled torques or displacements to the joints. Providing this array of sensors and actuators to all the muscles and joints is very difficult, so that our initial efforts, reported in this study, are performed on a reduced-scale version of the arm having only the elbow flexion-extension degree of freedom with an attached optical encoder position sensor and a torque motor.

The physical elbow system has several mechanical properties which are very close to those of the human arm: (1) McKibben pneumatic actuators (Schutte 1961; Chou and Hannaford 1996) were used as elbow flexor and extensor. (2) Force sensors which act as Golgi tendon organ (GTO), and mechanical muscle spindles which mimic the behavior of biological muscle spindles (Marbot and Hannaford 1993; Marbot 1995), are integrated in the system. (3) The shape of the limb segment and the attachment points of the muscles were chosen based on human anatomical geometry (Snell 1980; Zuckerman and Matsen 1989) to mimic the real human forearm mechanical properties around the elbow joint. Finally, the physiologically analogous artificial neural network controller (Hannaford et al. 1995) is implemented to emulate the behavior of spinal segmental reflex circuitry (Binder 1989a, b).

However, there are two major limitations of our system: (1) Since the large number of motor units in a biological muscle are emulated in our system by only one artificial muscle and motoneuron, phenomena related to motor unit recruitment can not be studied. (2) Since only one sensor of each type is used for each muscle, spatial summation of multiple afferent signals will not take effect.

There are three key reasons for using a physical arm instead of a mathematical model: (1) A physical system will obey all physical laws which otherwise may be neglected or may not even be considered when modeling. (2) While we can build a physical arm with mechanics as close as possible to human arm, the complexity of a mathematical model which implements similar details of mechanics will make it very difficult to simulate. (3) The implementation of the physical anthropomorphic arm itself may help develop new technologies for novel actuators, sensors, and prosthetic arms.

The reduced dimensionality of the testing elbow system makes it relatively more amenable to computer simulation. However, the intention of the testing elbow construction is to validate models, technologies, and control parameters for eventual incorporation into the full, multi-degree of freedom arm. To transfer knowledge to our more complex spatial arm, we cannot rely on computer simulation of the elbow system.

In the following, we begin by describing the general experimental setup. Then, four groups of experiments will be described, which include (1) open loop stiffness control with muscle co-contraction, (2) simple closed loop stiffness control with Ia afferent or Ib afferent feedback, (3) posture maintenance with spinal reflex circuitry in response to transient perturbation, and (4) experiments in which spinal reflex circuit elements are artificially modified.

The four experiments are aimed at testing the hypothesis that a technological arm can be built which has dynamic response comparable to the human arm as measured in comparable experiments. Given such a response, we would also like to modify the system experimentally and observe the effects of these alterations on performance.

Although the literature on reflex performance around the human elbow joint is far from complete, the third experiment will compare performance of the elbow system with a physiological experiment performed by Lacquaniti et al. (1982). A 'covariance diagram' will be introduced to visualize the large amount of experimental data and to highlight the phenomena of interest. Finally, the system behavior will be analyzed with reference to a linearized model, where by utilizing the flexibility and repeatability of the system, the specific roles of neural circuit elements will be identified and some nervous system abnormalities will be predicted.

2 Elbow test bed setup

The elbow test bed includes the elbow system, which is subdivided into the Neural Controller and the Testing Elbow, and a dynamic testing system (Fig. 1). The Neural Controller is implemented by a real-time artificial neural network program in a digital signal processor (DSP) based computer (Hannaford et al. 1995). The Testing Elbow consists of an equivalent limb segment and two McKibben muscles (pneumatic actuators) (Chou and Hannaford 1994, 1996) each attached in parallel with a mechanical muscle spindle (Marbot and Hannaford 1993; Marbot 1995) and force sensor. The two McKibben muscles act as elbow flexor and extensor. Electrical control signals are sent from the DSP controller, and sensory signals are fed back to the controller. The dynamic testing system consists of a personal computer (PC), a torque motor, an angular position optical encoder, and various sensors (some of which are overlapped with the elbow system). The PC performs mechanical data acquisition and feedback control of the torque motor if desired.

While the PC performs mechanical data acquisition, the DSP itself performs neural activities data acquisition. The efferent signals sent to the McKibben muscles are assumed to have the same timing and relative amplitude characteristics as a spatial summed and rectified electromyogram (EMG). The activities of the neural network elements and forearm mechanical variables were recorded during experiments and will be shown and analyzed in the following sections.

3 Experiments

3.1 Open loop stiffness control with muscle co-contraction

In this experiment, the actuator pressure (analogous to muscle activation level) was kept as constant as possible

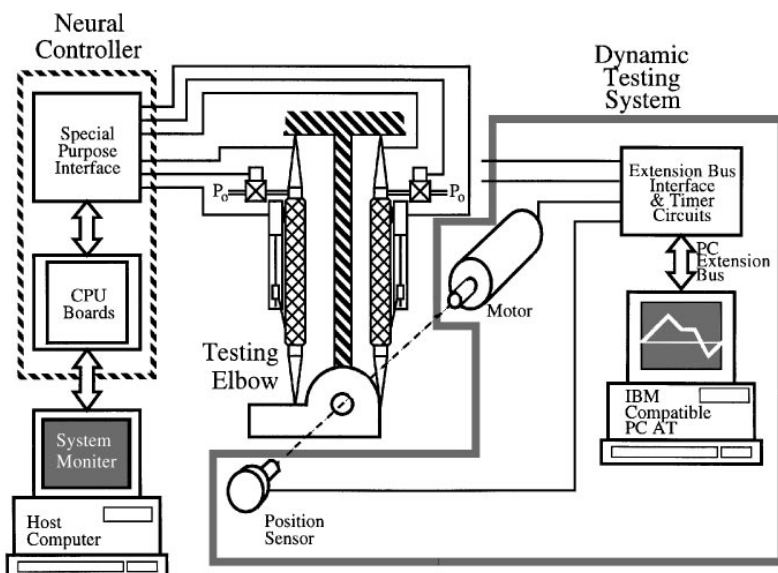


Fig. 1. Elbow test bed setup, including Neural Controller, Testing Elbow, and dynamic testing system

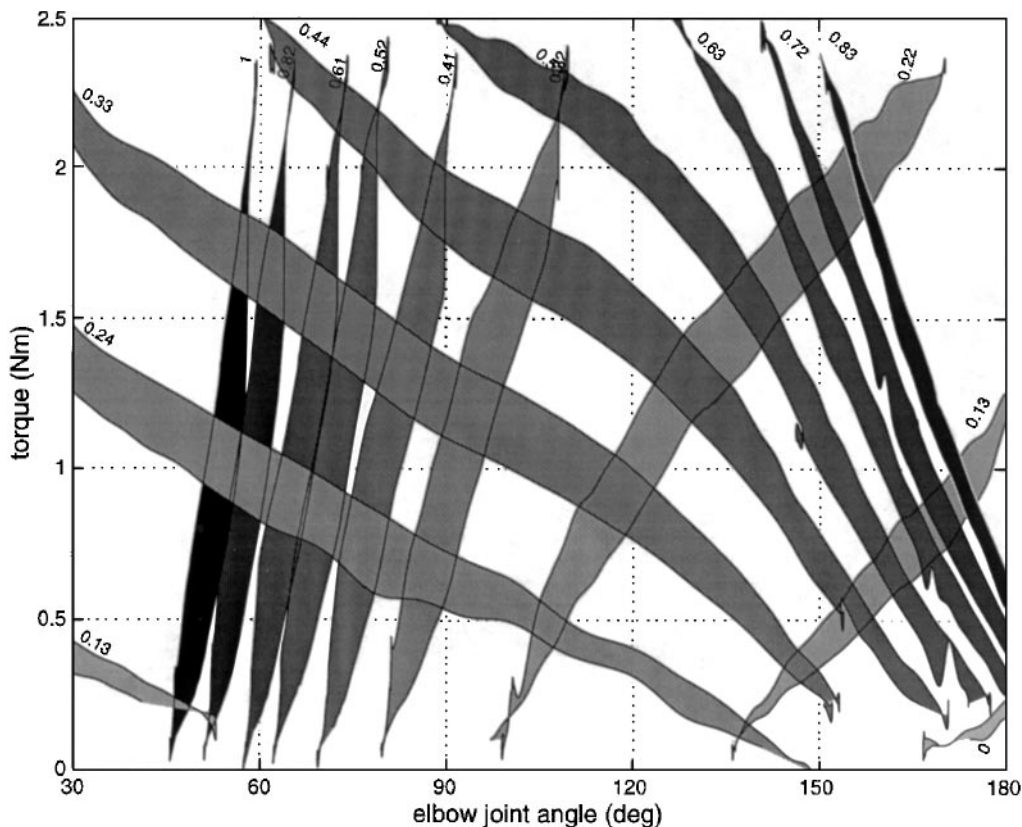


Fig. 2. Open loop torque-angle-activation relationships for elbow flexor and extensor. Joint equilibrium angle is the intersection of two curves, one for each actuator of corresponding activation level. Normalized muscle activation level is indicated on top of each curve with 1 corresponding to 100 psi (6.9 bar). Joint stiffness, which is the sum of stiffness of two muscles, increases when muscles co-contract

while cyclic displacement or torque patterns (0.25 Hz) were applied to the joint. The Neural Controller was not involved at this point. The relationships between elbow joint torque, displacement, and actuator pressure of the flexor and the extensor are superimposed in Fig. 2. The hysteresis loop of each curve is caused by the actuator friction and the gas viscosity. The loop direction is clockwise for flexor and counterclockwise for extensor. The joint equilibrium angle will be the intersection of two curves, one for each actuator of corresponding activation level. The stiffness (absolute value of the slope) of each actuator curve increases when the pressure increases. As a result, the joint stiffness, which is the sum of the stiffness of the two muscles, increases when muscles co-contract.

To verify the above point, constant-amplitude disturbing torque steps were applied to the elbow with various levels of co-contraction. The angular position was recorded and histograms of the position responses are shown in Fig. 3. The higher the co-contraction level, the narrower the histogram of position. This indicates that the stiffness increases with co-contraction.

3.2 Closed loop stiffness control with Ia or Ib afferent feedback

In this experiment, muscle spindle Ia afferent feedback and GTO Ib afferent feedback effects will be demonstrated.

The muscle spindle Ia afferent is sensitive to the length and velocity of human muscle (Binder 1989a). This

kind of feedback pathway to muscle activation will increase the stiffness of the mechanical system. The mechanical muscle spindle has been reported to be able to emulate the sensitivity and some nonlinear properties of the spindle under isolated testing (Marbot and Hannaford 1993; Marbot 1995). In this experiment, it will be tested with the flexor actuator of the arm to demonstrate the effect of joint stiffness modification.

In the first part of this section, the Neural Controller consists of an α motoneuron (α MN), a γ motoneuron (γ MN), and a Ia afferent sensory neuron. Each simulated 'neuron' actually represents a pool of physiological neurons. Values for the synaptic weight between Ia and α MN and a constant command signal to the α MN were chosen to achieve the desired operating points to keep the elbow motion in the dynamic region. The joint angle was recorded while a cyclic disturbing torque was applied to the elbow joint (Fig. 4). Each curve corresponds to a different synaptic weight of the Ia- α MN synapse. The relationships between joint stiffness and synaptic weight are plotted in the inset of Fig. 4. The joint stiffness increases significantly from 1.4 to 6.6 N m/rad when the synaptic weight increases.

On the other hand, the GTO senses the tension of its connected muscle fibers (Binder 1989a). The action of this kind of inhibitory feedback pathway will increase the compliance (reciprocal of stiffness) of the system. A strain gauge force sensor was applied to the 'tendon' of each actuator to perform this function.

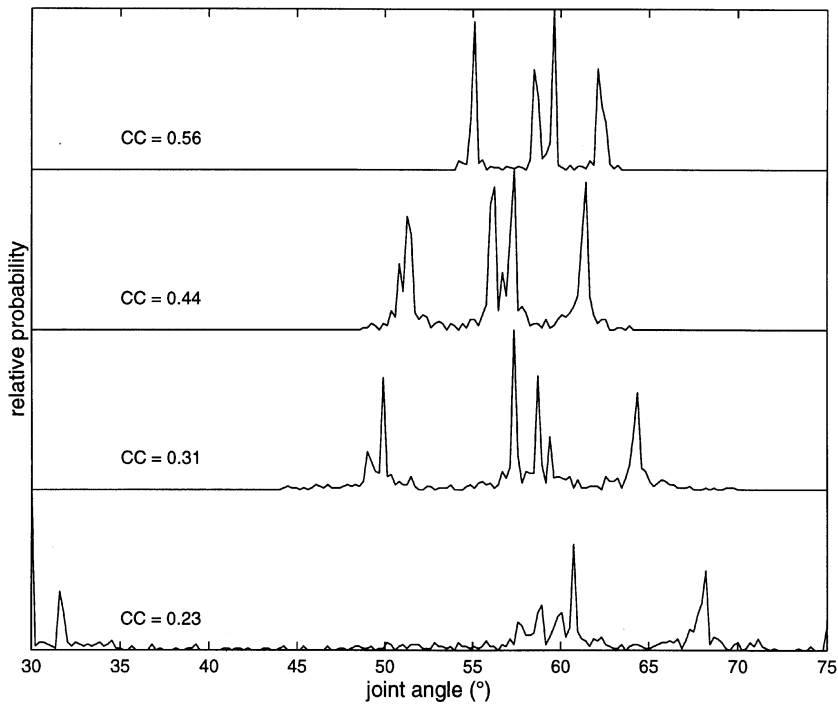


Fig. 3. Elbow joint angle histograms in response to constant-amplitude disturbing torque steps with different muscle co-contraction levels (CC). Narrower width of the histogram indicates joint stiffness is higher

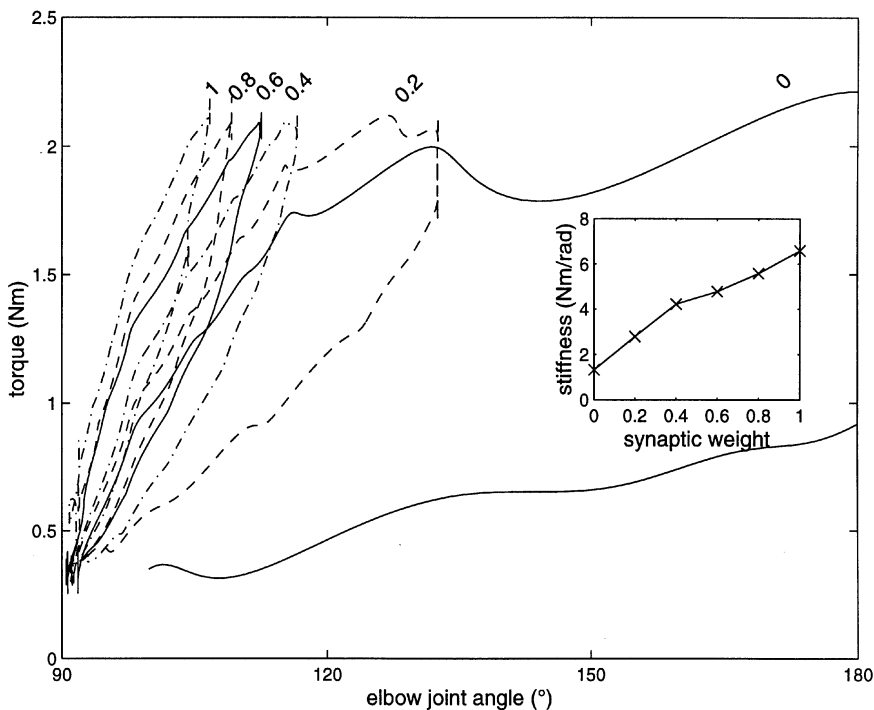


Fig. 4. Ia afferent effect. Joint angle was recorded while cyclic disturbing torque was applied to the elbow joint. Each *curve* corresponds to a different weight of the Ia- α MN synapse. Approximate stiffness versus synaptic weight is plotted in the *inset*. Joint stiffness increases significantly when synaptic weight increases

In the second part of this section, the neural network consists of an α MN, a Ib afferent sensory neuron, and a Ib inhibitory interneuron (IbIn). Values for the synaptic weight between IbIn and α MN and a constant command signal to α MN were again chosen to achieve the desired operating points. The joint torque was recorded while a cyclic disturbing angle was applied

to the elbow joint (Fig. 5). Each curve corresponds to a different synaptic weight of the IbIn- α MN synapse. The relationships between joint stiffness and synaptic weight are plotted in the inset of Fig. 5. The joint compliance increases significantly from 0.2 to 2 rad/Nm when the Ib inhibitory synaptic weight increases.

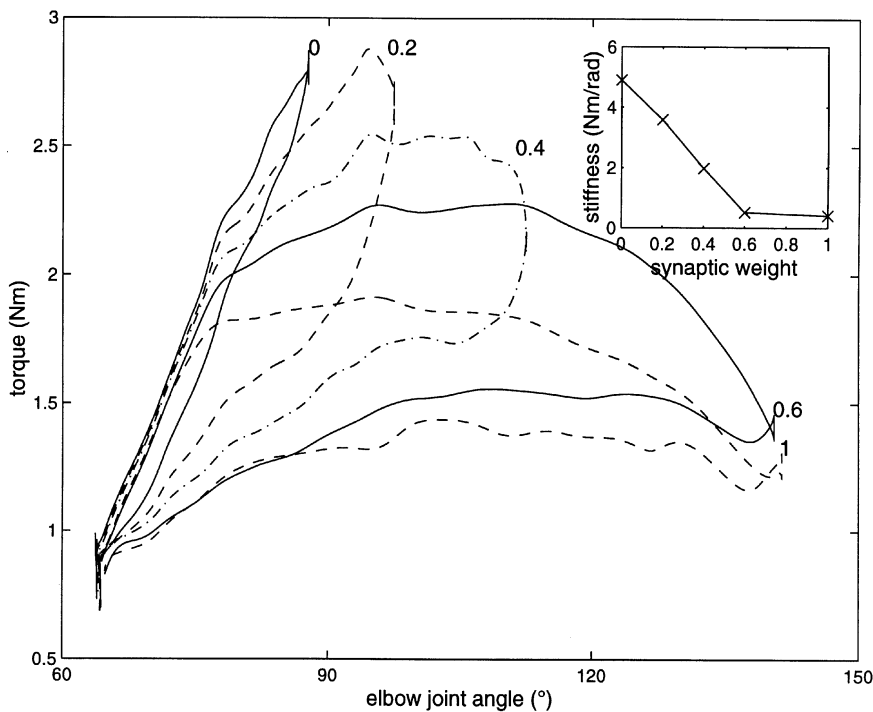


Fig. 5. Ib afferent effect. Joint torque was recorded while a cyclic disturbing angle was applied to the elbow joint. Each curve corresponds to a different weight of the IbIn- α MN synapse. Approximate stiffness versus synaptic weight is plotted in the inset. Joint stiffness decreases significantly when synaptic weight increases

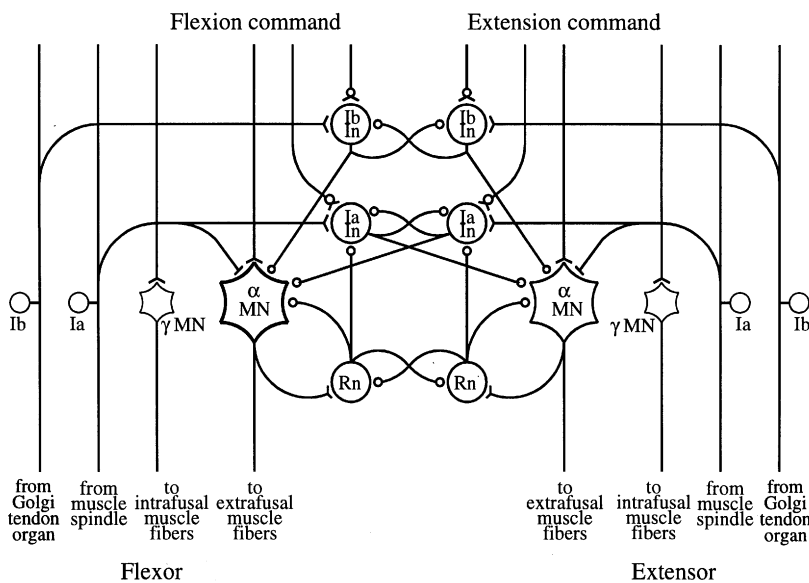


Fig. 6. Neural reflex circuitry of the spinal segment. Circuitry consists of α and γ motoneurons (MN), Ia and Ib afferents, Ia inhibitory (IaIn) and Ib inhibitory (IbIn) interneurons, and Renshaw cells (Rn), with descending pathways connected to all MNs and interneurons. Terminals with line segments or open circles represent excitatory and inhibitory synapses respectively. A combination of the above symbols (descending inputs) indicates pathways which may include more than one type of presynaptic neuron

3.3 Posture maintenance with spinal reflex circuitry in response to transient perturbation

A more complex neural network, based on human spinal segmental circuitry (Binder 1989a, b), is used in this experiment. The spinal segmental circuitry is believed to play the major role in the low-latency reflex response which, for example, is involved in posture maintenance against external perturbation (Fuchs 1989). The network in the DSP controller for this experiment consists of α MNs and γ MNs, Ia and Ib afferents, Ia inhibitory (IaIn) and Ib inhibitory (IbIn) interneurons, and Renshaw cells (Rn), with descending pathways connected to all MNs

and interneurons (Fig. 6). The software architecture allows each type of neuron to have an individually defined function to control its behavior, and each individual neuron can have its own set of parameters to fine-tune its response based on physiological evidence if available.

The testing conditions are designed to resemble those described in Lacquaniti et al. (1982), which demonstrated how different instructions to human subjects shape the reaction to the same external mechanical load and perturbation. In their experiment, the subject's upper arm was fixed, and the forearm was fitted with damped springs to create viscoelastic loads with three different

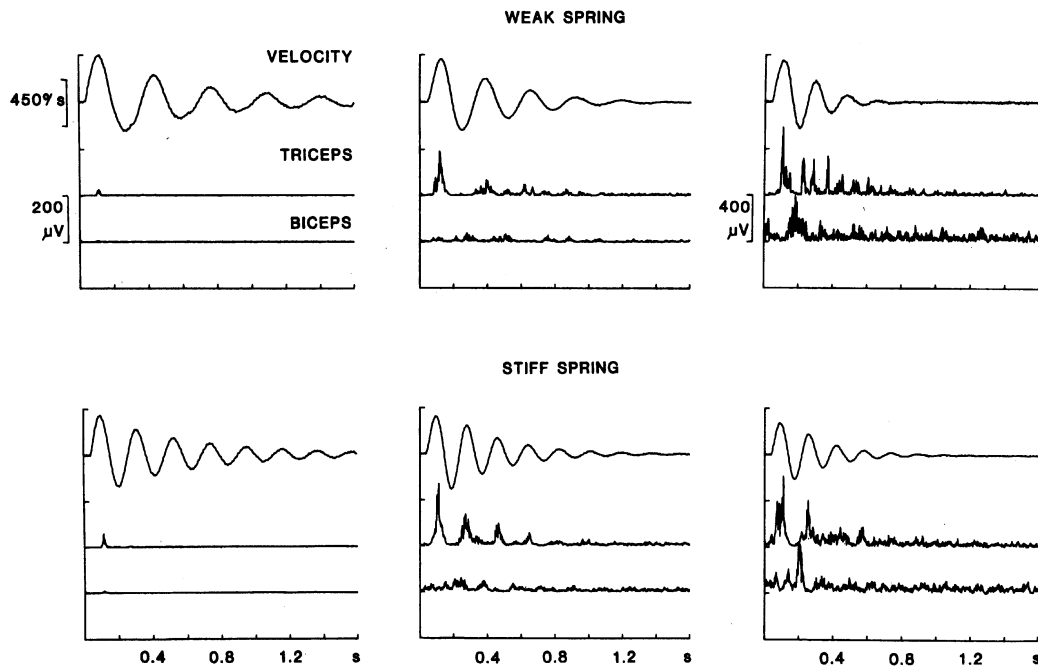


Fig. 7. Experimental results of Lacquaniti et al. (1982). *Left-hand column* corresponds to the task 'do not resist', *middle column* to 'resist', and *right-hand column* to 'resist maximally.' *Top trace* in each subplot corresponds to forearm angular velocity (flexion is positive); *middle* and

bottom traces are rectified electromyogram (EMG) activities of triceps and biceps, respectively. Perturbation responses were measured with three external viscoelastic loads. From Lacquaniti et al. (1982), with permission

values. Initially, the forearm and damped spring system was pulled away from its equilibrium angle by a torque motor. Then it was abruptly released and made damped oscillations. The subjects were instructed to perform three motor tasks: (1) 'not to resist the perturbations by remaining as relaxed as possible' (referred to as 'do not resist'), (2) 'to apply a moderate amount of force without attempting to control the perturbed position of their forearm' (referred to as 'resist'), and (3) 'to resist the perturbations so as to arrest the forearm oscillations' (referred to as 'resist maximally'). The results of their experiments showed that the estimated time constant decreases, and the stiffness, damping factor and oscillation frequency increase, when the instructed resistance level increases. In another words, the settling time is shorter when the resistance level is higher (Fig. 7).

To emulate the different instructions to subjects the following inputs were applied as 'descending commands' to our spinal level network. For the first motor task ('do not resist'), the descending commands of both α MNs and γ MNs were set to zero to emulate the 'relaxed' condition. For the Second task ('resist'), a moderate level of co-contraction command was applied to α MNs and γ MNs to produce 0.6 N m co-contraction torque from each, oppositely acting, muscle actuator. For the third task, since there was only spinal segmental control level in our system, intentional control to arrest the forearm oscillations is not possible. To substitute this case, a co-contraction level of 1.5 N m was chosen (referred to as 'resist harder') to obtain higher resistance without intention.

The viscoelastic load was emulated by the closed loop controlled torque motor with three different position and velocity feedback gains to produce stiffness and damping equivalent to the damped springs used in the experiments of Lacquaniti et al. (1982). Note that the medium load has the lowest value of viscosity among the three. Tests without load were also performed for comparison.

As in Lacquaniti et al.'s experiment, the forearm and damped spring system was initially pulled away from its equilibrium angle and then abruptly released making damped oscillations. The transient elbow joint velocity and actuator valve input signals (EMG) are shown in Fig. 8. Each column corresponds to a different motor task: i, 'do not resist'; ii, 'resist'; and iii, 'resist harder.' Each row corresponds to a different viscoelastic load: 0, no load; 1, weak spring; 2, medium spring; and 3, stiff spring. The parameters of the oscillation (time constant, stiffness, damping factor) were calculated from the first four wavelengths of each oscillation. The time constant decreased, and the stiffness, damping factor, and oscillation frequency increased, when the commanded resistance level increased (Chou 1996). This matches the results of Lacquaniti et al.'s (1982) experiment very well. However, in the 'resist harder' task, the computed time constant did not decrease as significantly as it did in the 'resist maximally' task of Lacquaniti et al.'s experiment. This will be discussed in more detail later.

The test system allows all neural activities, afferent and efferent signals, and dynamical variables to be recorded. Although complete sets of data were recorded in this experiment, the amount of data is too large to report

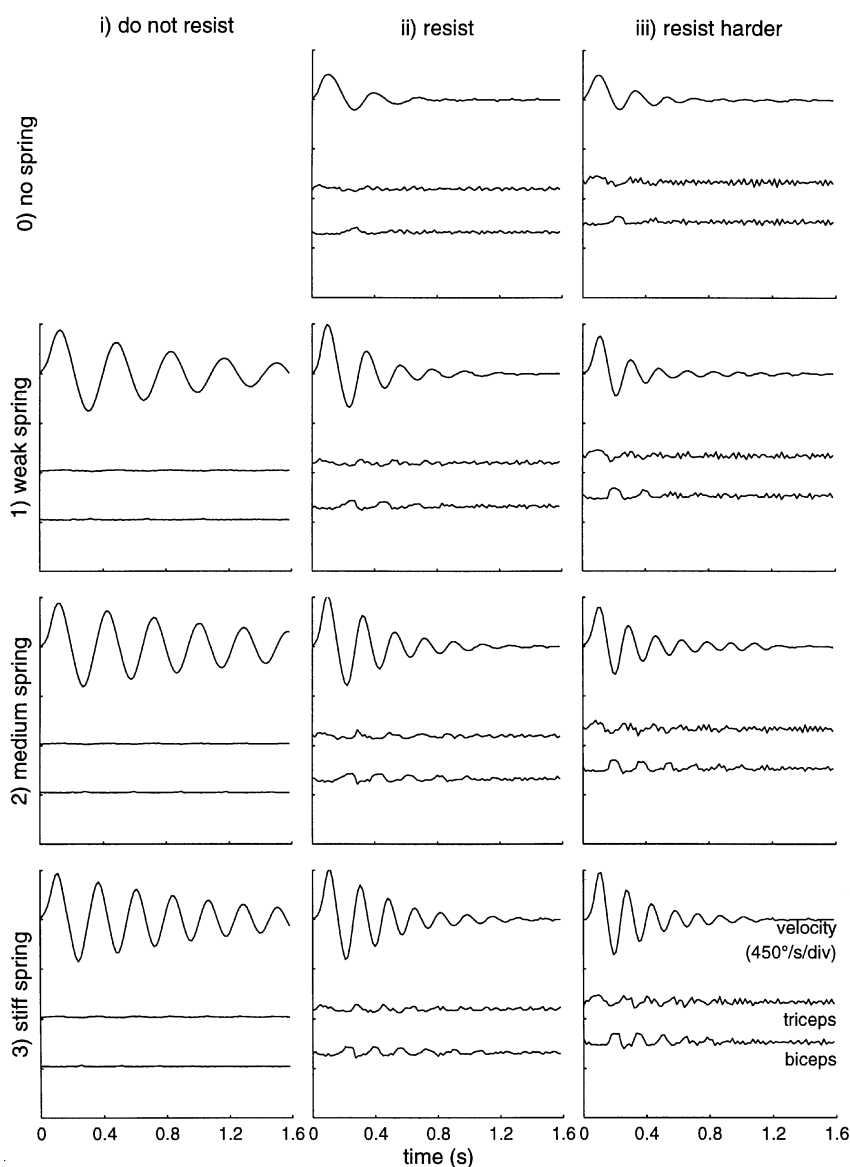


Fig. 8. Artificial elbow joint transient response with spinal reflex circuitry. Each *column* corresponds to a different task: i, 'do not resist'; ii, 'resist'; and iii, 'resist harder.' Each *row* corresponds to different viscoelastic load: 0, no load; 1, weak spring; 2, medium spring; and 3, stiff spring. *Top trace* in each subplot corresponds to forearm angular velocity (flexion is positive); *middle and bottom traces* are analogous to spatial summation of rectified EMG activities of extensor and flexor muscle groups, respectively

in this article. Instead, the covariance coefficients of each pair of variables are plotted as circles in a matrix (Fig. 9). The size of the circle represents the amplitude of covariance between the row and column variables, and black indicates positive. We will call this a covariance diagram. The covariance diagram greatly reduces the amount of data and highlights the points of interests.

By properly arranging the order of the variables, the covariance diagram forms several clusters with large circles and others with small circles. The clusters of larger circles indicate that the variables in the cluster are strongly related to each other (e.g., Ia, IaIn, Rn, and α MN to each other). The clusters of small circles indicate that the variables in the cluster are weakly related to each other (e.g., Ib and IbIn are weakly related to Ia, IaIn, Rn, and α MN). Also, we can find that the positively covarying pairs are mostly located near the diagonal, while

the negative ones are located near the anti-diagonal. This demonstrates the agonist-antagonist nature of the system (e.g., the flexor α MN cluster and the extensor α MN cluster). On the diagonal itself are trivial covariances of +1. Figure 9 plots the covariances for the 'medium' spring and the 'resist' instruction. The covariance diagrams for the other conditions looked quite similar (Chou 1996).

3.4 Comparative experiments with modified spinal reflex circuit elements

In order to highlight the roles of specific subnetworks of the neural circuitry, another set of experiments were performed similar to the above but with modified neural circuitry. The following configurations, modified from the original circuitry (Fig. 6), were chosen: (1) without

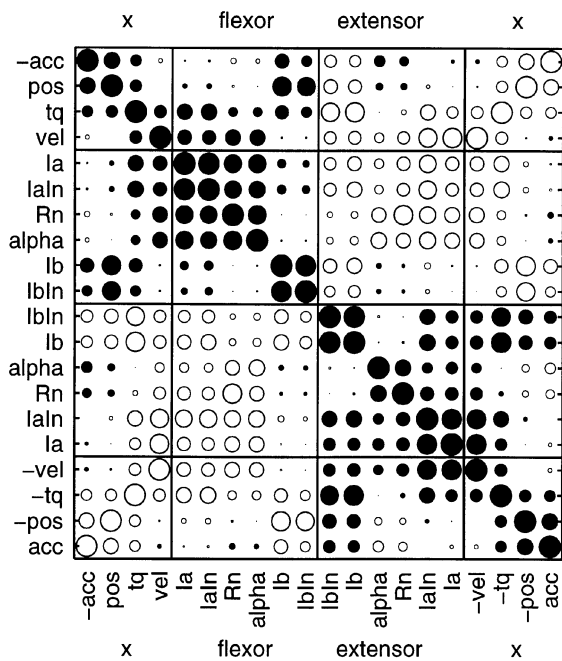


Fig. 9. Covariance diagram of experiment with spinal reflex circuitry. Covariance coefficients of each pair of variables, including neural activities and elbow joint mechanical quantities, are plotted as circles. The size of a circle represents amplitude of covariance between row and column variables, and color represents sign (black is positive, white is negative). Activity covariances are plotted for the case of the 'medium' spring with the 'resist' instruction

γ dynamic excitation of muscle spindles, (2) without Ia feedback, (3) without Ib feedback, (4) without Ia or Ib feedback, and (5) without α MN activation dynamics.

The transient responses are shown in Fig. 10. Each column corresponds to a different motor task: ii, 'resist' and iii, 'resist harder.' Each row corresponds to a different network configuration: 3a, without γ MN dynamic excitation; 3b, without Ia afferent feedback; 3c, without Ib; and 3d, without Ia or Ib. Only the trials with the stiff spring are performed. The result of the tests without α MN activation dynamics was very similar to that of the tests without γ dynamic excitation and is not shown. In general, the results show that the system stiffness decreases without Ia feedback, and increases without Ib feedback. Also, the damping factor decreases without either γ dynamic excitation or α MN dynamics. None of these modified configurations can obtain the same disturbance rejection performance (short time constant) as the original network.

The covariance diagram introduced in the previous section is applied here also and is shown in Fig. 11 for each experimental modification to the system. The column and row numbering is as defined in Fig. 10. To calculate the covariance, afferent signals were always recorded even if feedback was turned off. For convenience, neurons are classified into three subsystems: α subsystem; including α MN and Renshaw cell; Ia subsystem, including Ia afferent and IaIn; Ib subsystem, including Ib afferent and IbIn. Compared with the previous

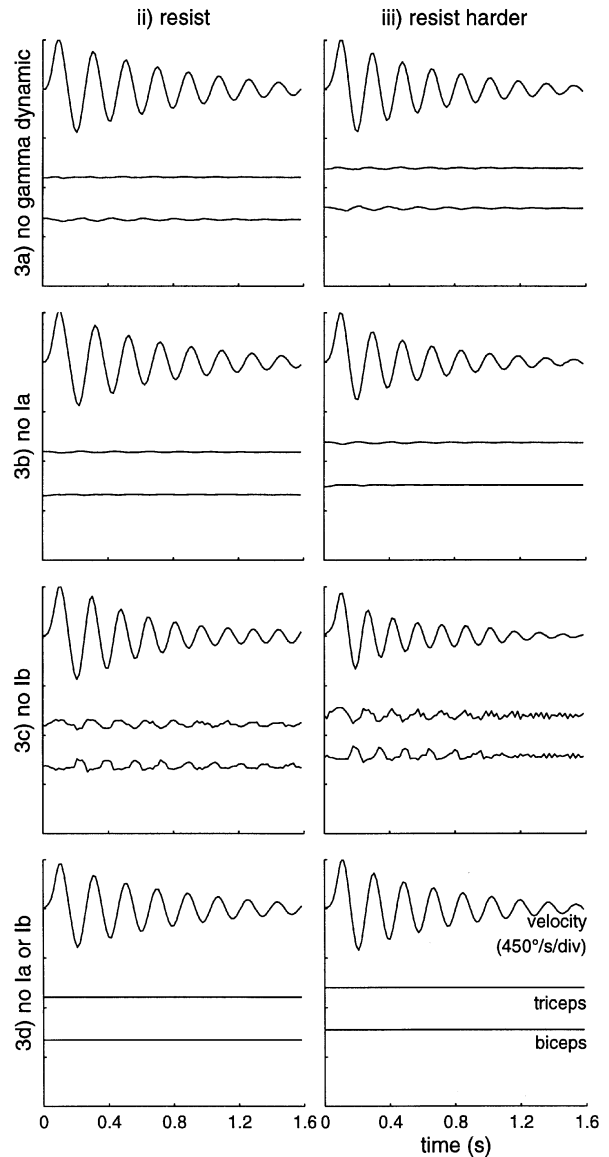


Fig. 10. Elbow joint transient response with modified circuitry. Each column corresponds to different motor tasks: ii, 'resist'; and iii, 'resist harder.' Each row corresponds to a different, modified, network configuration: 3a, without γ MN dynamic excitation; 3b, without Ia afferent feedback; 3c, without Ib; and 3d, without Ia or Ib. Only the trials with the stiff spring are performed. The top trace in each subplot corresponds to forearm angular velocity (flexion is positive); the middle and bottom traces are equivalent to average rectified EMG activities of extensor and flexor muscle groups, respectively

experiment, only the configuration without Ib feedback has similar covariance diagram patterns. The one without γ dynamic excitation has strong covariance between Ia, Ib, and α subsystems. The case without Ia feedback has very low covariance between Ia and α subsystems but very strong (negative) covariance between Ib and α subsystems. Finally, the case without either Ia or Ib subsystem has very low covariance between different subsystems, and most off-diagonal circles shrink into small dots.

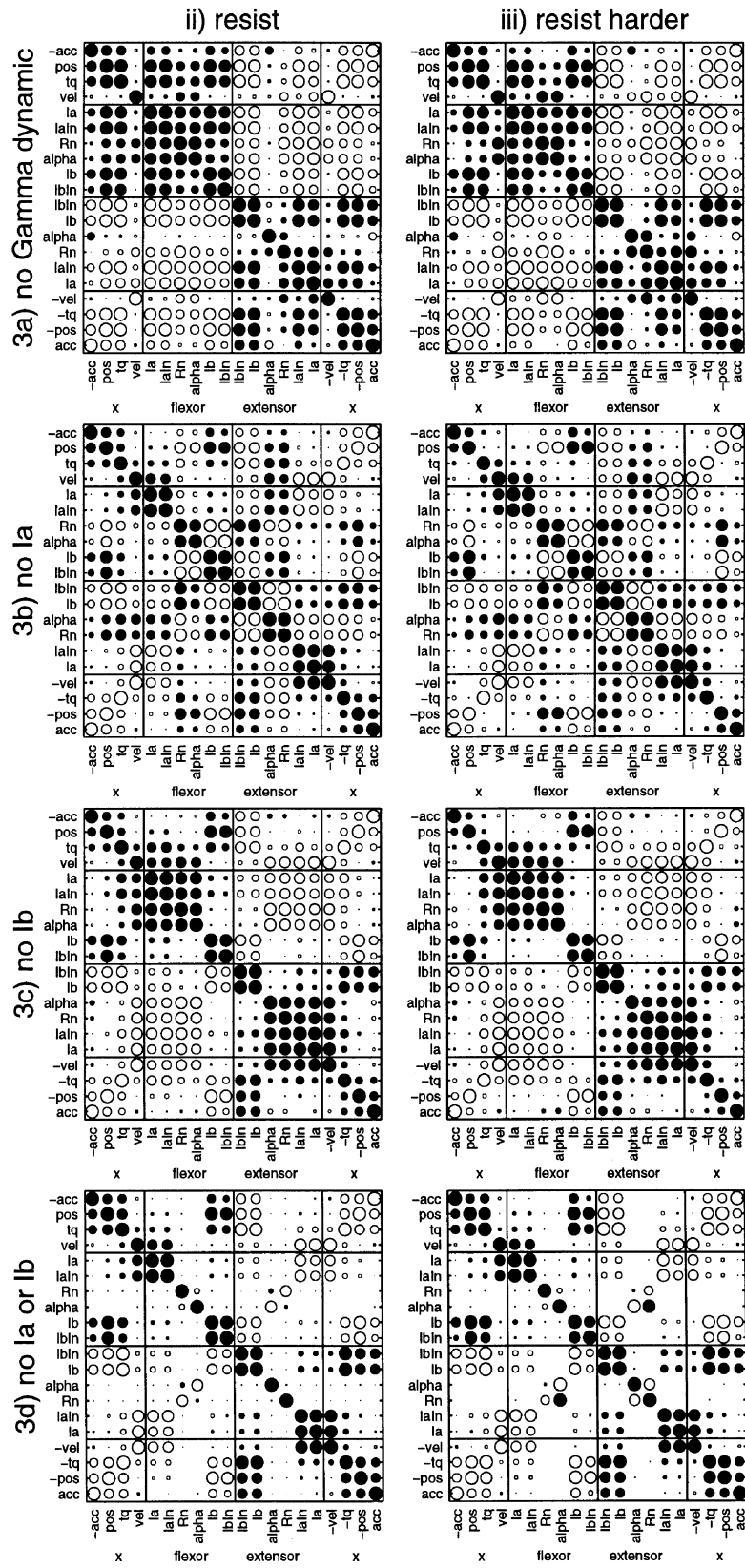


Fig. 11. Covariance diagrams of experiment with modified circuitry. Covariance coefficients of each pair of variables are plotted as in Fig. 9. *Notation* and column and row numbering are as defined in Fig. 10

4 Discussion

4.1 Tools

In the following, we will explain the effects of the system components and the loads from a linear control point of view. This linear model will help us clarify the relative roles of co-contraction and Ia reflex activity in maintaining posture. Although the system is nonlinear, a linear model can be used to qualitatively analyze the effects of some system parameters and to conveniently show plausible roles for system components in generating the observed experimental results. Of course it should always be kept in mind that the accuracy of the linear model will decrease significantly when system states are moving away from the current operating point.

The signal block diagram of the system, including the controller, G , the plant, P , and the feedback, H , are shown in Fig. 12. The frequency response from the closed loop joint angle to the perturbing torque will be:

$$\frac{X(s)}{F_L(s)} = \frac{P(s)}{1 + G(s)P(s)H(s)} \quad (1)$$

In terms of linear analysis, the frequency response of the α MN and muscle activation dynamics can be approximately expressed as:

$$G(s) = \frac{F_m(s)}{E(s)} = \frac{K_m(x_0 - x)(1 + s/z)}{1 + s/p} \quad (2)$$

where F_m is muscle torque, E is α MN input, K_m is muscle stiffness, x_0 is joint angle at ideal minimum muscle length, z is α MN activation dominant zero, and p is muscle activation dominant pole. The joint angle, x , is treated as a constant in this equation (as in the isometric case) for simplicity. Note that the term ‘muscle’ implies extrafusal muscle fiber if not specified elsewhere. The effect of propagation delay is not covered in the linear model. However, realistic delays (17 ms reflex from sensors to actuators mechanical response time) were built into the afferent and efferent links in the physical elbow system.

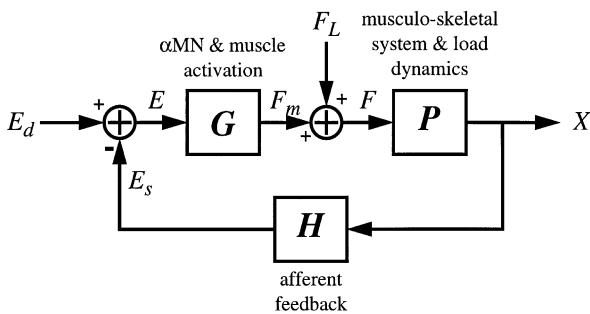


Fig. 12. Signal block diagram of simplified elbow joint linear model, which includes the controller, G , plant P , and feedback, H

The frequency response of the arm and load dynamics (the plant) is

$$P(s) = \frac{X(s)}{F(s)} = \frac{1}{(K_m a_m + K_L) + (B_m a_m + B_L)s + (I_{arm} + I_L)s^2} \quad (3)$$

where X is joint angle, F is total torque, K_m is muscle stiffness, B_m is muscle viscosity, I_{arm} is forearm inertia, K_L is load stiffness, B_L is load viscosity and I_L is load inertia. The normalized muscle activation level, a_m , is treated as a constant in this equation, again for simplicity. Note that the muscle internal length-tension and tension-velocity relationships are treated as individual elastic and damping elements in the plant.

The frequency response of the muscle spindle afferent feedback is

$$H(s) = \frac{E_s(s)}{X(s)} = wr(K_s a_s + B_s a_s s) \quad (4)$$

where E_s is Ia afferent feedback output, w is synaptic weight to α MN, r is a scaling factor, K_s is spindle stiffness, B_s is spindle viscosity and a_s is normalized spindle activation level. The effect of Ib afferent feedback can be analyzed in the same manner.

The relationships X/F_L , P and $1/GH$ are shown schematically in Fig. 13, assuming that the zero of α MN activation dynamics matches the pole of muscle activation dynamics. According to (1), the value of X/F_L will approximate P if P is much less than $1/GH$ (i.e., GPH is much less than 1, typically in the high-frequency range), and approximate $1/GH$ if P is much greater than $1/GH$ (i.e., GPH is much greater than 1, usually in the medium- and low-frequency range). In addition, it will be less than either P or $1/GH$ if the phase of GPH is away from 180° . In other words, the X/F_L curve is upper bounded by and very close to the P or the $1/GH$ curve, whichever is smaller.

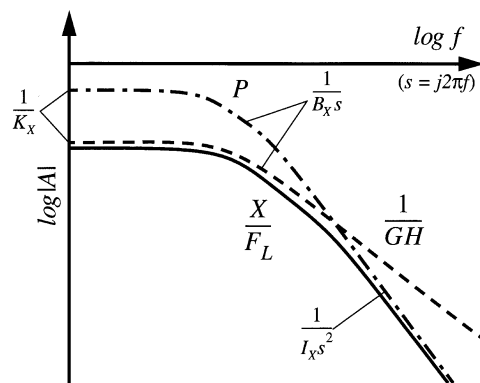


Fig. 13. Schematics of elbow joint frequency response. The X/F_L curve (limb compliance) is upper bounded by and very close to the P or $1/GH$ curve, whichever is smaller

4.2 Load effects

Viewed in the frequency domain, the arm and load dynamics described in (3) (Fig. 13, curve P) forms three segments with slopes of 0 dB/dec (decade), -20 dB/dec, and -40 dB/dec, respectively. External stiffness and damping were supplied in Lacquaniti et al.'s experiment and are included in our model. Increasing external load stiffness will reduce the magnitude of the 0 dB/dec segment and, as a result, decrease the system damping factor and increase oscillation frequency. This can be verified by comparing row 1 with row 3 in Fig. 8. Similar changes appear in Lacquaniti et al.'s results (Fig. 7).

Increasing external load viscosity will reduce the magnitude of the -20 dB/dec segment and increase the system damping factor. This can be verified by comparing Fig. 8, row 2 (with the smallest damper) with row 1 and row 3. Finally, increasing load inertia will reduce the magnitude of the -40 dB/dec segment, and decrease system damping factor and oscillation frequency (this effect is not studied in the experiments).

4.3 Open loop co-contraction effects

When subject to open loop co-contraction, the intrinsic stiffness and viscosity of muscle have mechanical effects similar to those described above. However, in biological muscle, the changes in viscosity and stiffness are dependent and usually proportional to each other. Under this constraint, without a significant change in inertia, the damping factor will increase when the co-contraction level increases. In addition, because the initial external perturbations in the 'posture maintenance' experiment were chosen to have the same amplitude of displacement regardless of the system stiffness, the effect of stiffness on steady-state position error can not be observed in the results. However, in the 'open loop stiffness control' experiment, it is obvious that by applying constant amplitude torque perturbations, the steady-state position error will be smaller when joint stiffness increases by muscle co-contraction (Fig. 3). This is also true with afferent feedback and is also consistent with the linear model. As a result, co-contraction is an effective way not only to reduce the steady-state error of joint angle but also to reduce the settling time (proportional to the time constant) of the system. The effect on settling time is shown by comparing Fig. 8, 3.i with Fig. 10, row 3d. The time constants decrease from 1.13 s to 0.64 s as co-contraction level is increased.

4.4 Ia and Ib afferent effects

According to (2) and (4) the $1/GH$ curve in Fig. 13 forms two segments with slopes of 0 dB/dec and -20 dB/dec respectively. As mentioned in Sect. 4.1, the X/F_L curve will approximate the $1/GH$ curve in the low- and medium-frequency range, and approximate the P curve in the high-frequency range. Similar to the effect of open loop co-contraction on the P curve and closed loop response, increasing the spindle stiffness and viscosity (by increasing the γ excitation level) is an alternative way to

reduce the steady-state error of joint angle and the system time constant. The effect of Ia afference with γ excitation on settling time is shown by comparing Fig. 8, row 3 with Fig. 10, row 3b. By applying the Ia afference with α - γ co-activation, the results yield time constants of 0.37 and 0.29 s (Fig. 8, 3.ii and 3.iii). By removing the Ia afference, which is equivalent to deactivating γ MN, with only α co-contraction, the results yield time constants of 0.64 and 0.49 s (Fig. 10, 3b.ii and 3b.iii). This effect is also shown by comparing row 3c with row 3d in Fig. 10, where Ia afference yields time constants of 0.57 and 0.40 s (Fig. 10, 3c.ii and 3c.iii), and without Ia afference yields time constants of 0.72 and 0.64 s (Fig. 10, 3d.ii and 3d.iii).

By combining open loop co-contraction and Ia afference with γ excitation, the system performance greatly increases in terms of steady-state error and settling time. This is shown by comparing 'do not resist' cases in Fig. 8, column i, with 'resist' and 'resist harder' cases in columns ii and iii. The time constants significantly decrease at each load when the α - γ co-activation levels increase (see Chou 1996, for numerical values and parameter fitting procedure).

Two major differences between the Ia afferent effect and open loop co-contraction effect are efficiency and stability. The muscle activity produced by Ia afferent feedback is only induced when there is a perturbation, while co-contraction activity is always present. This makes Ia afferent feedback more efficient than muscle co-contraction since isometric co-contraction uses a lot of metabolic energy without doing any work. On the other hand, Ia afferent feedback is subject to phase lag due to neural conduction delay. Although we do not cover the effect of feedback time delay in the linearized model, delay, as is present in both the biological and anthropomorphic arms, limits the maximum feedback gain (and, in turn, the closed loop stiffness and viscosity) possible at a given phase margin. Time delay has no effect on the stability of the open loop system.

While Ia afferent feedback increases the closed loop stiffness, Ib afferent feedback decreases it. The system without Ib afference has higher stiffness, a lower damping factor, and a longer time constant. This is shown by comparing responses with Ib afference (Fig. 8, row 3 and Fig. 10, row 3b) with responses without Ib afference (Fig. 10, row 3c and row 3d).

Since the Ia and the Ib afferent systems have the opposite effect, how these two afferent systems cooperate remains to be determined. There are two reasonable suggestions. (1) Ia afferent feedback is utilized during position-priority tasks while Ib afferent feedback is utilized during force-priority tasks. (2) since Ia afferent and Ib afferent signals are not only processed by the spinal segmental reflex circuitry but also propagate through inter-segmental and higher CNS levels, they are very likely to be processed by other neural circuitries in different ways and have different effects.

4.5 Gamma static and dynamic excitation effects

The mechanical properties of intrafusal muscle fibers are controlled by the γ MN (Binder 1989a). While γ static

excitation mainly changes the stiffness of the fiber [(4) $K_s a_s$], γ dynamic excitation mainly changes the viscosity ($B_s a_s$, where the two a_s can be different). This allows the system to modify position feedback and velocity feedback independently through the Ia afferent. The difference in the resulting system response is shown by comparing Fig. 8, row 3 with Fig. 10, row 3a.

4.6 Dynamic characteristics of α MN and muscle activation

In previous discussion, the zero of α MN activation dynamics and the pole of the muscle activation dynamics were assumed to match each other. Shoemaker (1993; Shoemaker and Honnaford 1994) suggested an optimal value of the zero of -26.0 rad/s (-4.13 Hz) for the α MN activation dynamics. Although a cat's α MN was studied in her thesis, this value should be close enough to a human α MN for our experiments. On the other hand, the pole of muscle (actuator) activation dynamics can be derived from the reciprocal of the time constant of muscle (actuator) isometric activation. The time constant of our artificial muscle actuators was measured to be 45 ms, yielding a pole at -22.2 rad/s pole. This is close enough to achieve a good degree of pole-zero cancellation in our system.

The perturbation response of the elbow system without α MN activation dynamics was similar to the result without γ dynamic excitation (Fig. 10, row 3a). Since there is no longer an α MN zero to cancel the effect of the muscle pole (2) this pole in turn bends the medium- and high-frequency portion of the *GH* curve to flat (originally 20 dB/dec). In other words, the α MN activation dynamics has a feedforward effect to overcome the high-frequency attenuation and phase lag (lowpass filtering) of muscle activation dynamics. This helps to maintain stability with higher closed loop gains.

4.7 Additional factors

The results of our experiment (Fig. 8) are very consistent with the results of the experiment by Lacquaniti et al. (Fig. 7) except for the third motor task. Because of the lack of high-level response in our system, the two experiments are not directly comparable. We compensated for this lack of high-level response with increased co-contraction, and labeled the condition 'resist harder' in our setup compare with 'resist maximally' in their setup. The settling time does not decrease as significantly as it does in the 'resist maximally' task of Lacquaniti et al.'s experiment because of insufficient change of damping. In a recent study, the McKibben pneumatic muscle was found to have less damping than biological muscle (Chou and Hannford 1994, 1996). This is a major performance limitation to our physical elbow system. In addition, it is also very likely that the higher-level CNS has a time-varying strategy to utilize α MN co-activation and γ MN static and dynamic excitation. Both these areas are the objects of current efforts in further developing the arm system.

4.8 Covariance diagrams

It is not difficult to find a strong relationship between the network configuration (Fig. 6) and the covariance diagrams (Figs. 9, 11). An excitatory synapse with large synaptic weight will dominate the covariance of its pre- and postsynaptic neurons. This is shown by the strong covariance between the Ia afferent and the α MN (Fig. 9), which have an excitatory synapse with large synaptic weight, unless feedback is turned off deliberately (Fig. 11, rows 3b and 3d). On the other hand, an inhibitory synapse seems to have less effect on the covariance of its pre- and postsynaptic neurons if there are other excitatory sources sent to the postsynaptic neuron. This is shown by the weak covariance between the Ib afferent and the α MN (Fig. 9), which have an inhibitory synapse with the presence of Ia feedback. As a result, the absence of Ib feedback does not change the covariance much (Fig. 11, row 3c). However, if the inhibitory synapse becomes the only source for the postsynaptic neuron, it will in turn dominate the covariance of its pre- and postsynaptic neurons with a negative value. This is shown when the Ib afferent inhibits the α MN without the presence of Ia feedback. Finally, when both Ia and Ib feedbacks are turned off, the covariance between Ia, Ib, and α MN drops to some small value which depends on the pattern of movement.

It is interesting to note that Ia and Ib afferents become strongly co-varying when the γ dynamic excitation of the muscle spindle is absent (Fig. 11, row 3a). This might imply their high redundancy. However, this covariance will decrease if a variable descending command or different load pattern is given.

5 Conclusion and future work

In this paper the human-like performance of the Neural Controller and Testing Elbow has been successfully demonstrated in both open loop and closed loop conditions. In open loop conditions, joint stiffness was effectively controlled by muscle co-contraction. In simple closed loop conditions, joint stiffness increases significantly when the synaptic weight from Ia afferent to α MN increases, and decreases significantly when the synaptic weight from Ib inhibitory interneuron to α MN increases. By implementing a model of human spinal reflex neural circuitry in the controller, the elbow joint response to transient perturbation resembled experimental results in humans. Muscle co-contraction with afferent feedback greatly increased the system damping factor and shortened the settling time of the transient damped oscillation.

By utilizing the flexibility and repeatability of the Neural Controller, networks with modified synapses or neural activation dynamics were tested systematically to predict the results of experiments which are impossible to perform on human subjects. These tests also elucidated the roles of several synaptic connections and neurons. For example, the results reveal that γ dynamic excitation is essential to produce the velocity feedback of the Ia

afferent signal, which then effectively increases the closed loop damping factor. Second, the α MN activation dynamics works as a feedforward phase-lead controller to compensate the lowpass-filtering effect of muscle, and to maintain the system open loop bandwidth and phase in a closed loop controllable condition.

Finally, the covariance diagram was a useful method for visualizing relationships between large numbers of neurons and physical variables.

In the future it will be possible to extend the emulated neural circuitry to perform multi-joint tasks with an anthropomorphic robotic arm (Hannaford et al. 1995) (shoulder and elbow joints). However, due to the large number of synapses and neurons, a neural learning method will become more important for tuning the network parameters. A Hebbian type algorithm (Hebb 1949) may be the most desirable one, which can be easily integrated into the controller and can run in real time.

The implementation of higher-level feedforward and feedback control neural circuitries will cause greater difficulties. Physiological experimental data on these pathways are very rare (even from animals). However, substantial data are available from single-unit recordings (Fetz et al. 1989; Yetz 1993) and models (Borghese and Arbib 1995). The integration of this knowledge into a predictive model of movement, posture, and contact control will be a major role for physical replica models such as the anthropomorphic arm.

Acknowledgements. This work was supported by the US Office of Naval Research, grant number N00014-92-J-1401.

References

- Binder MD (1989a) Peripheral motor control: spinal reflex actions of muscle, joint, and cutaneous receptors. In: Patton H et al. (eds) Textbook of physiology, 21st edn, vol 1. University of Washington, School of Medicine, Seattle, Washington, chap 24
- Binder MD (1989b) Spinal and supraspinal control of movement and posture. In: Patton H et al. (eds) Textbook of physiology, 21st edn, vol 1. University of Washington, School of Medicine, Seattle, Washington, chap 26
- Borghese NA, Arbib MA (1995) Generation of temporal sequences using local dynamic programming. *Neural Networks* 8:39–54
- Bullock D, Contreras-Vidal JL, Grossberg S (1992) Equilibria and dynamics of a neural network model for opponent muscle control. In: Bekey G, Goldberg K (eds) *Neural networks in robotics*. Kluwer Academic, Boston, pp 439–457
- Chou CP (1996) Study of human motion control with a physiologically based robotic arm and spinal level neural controller. PhD dissertation, University of Washington, Department of Electrical Engineering
- Chou C-P, Hannaford B (1994) Static and dynamic characteristics of McKibben pneumatic artificial muscles. In: Proc IEEE Int Conf on Robotics and Automation, San Diego, Calif, May 1994, vol 1, pp 281–286
- Chou C-P, Hannaford B (1996) Measurement and modeling of McKibben pneumatic artificial muscles. *IEEE Trans Robotics and Automation* 12:90–102
- Fetz EE (1993) Cortical mechanisms controlling limb movement. *Curr Opin Neurobiol* 3:932–939
- Fetz EE, Cheney PD, Mewes K, Palmer S (1989) Control of forelimb muscle activity by populations of corticomotoneuronal and rubromotoneuronal cells. *Prog Brain Res* 80:437–449
- Fuchs AF (1989) Control of movement. In: Patton H et al. (eds) Textbook of physiology, 21st edn, vol 1. University of Washington School of Medicine, Seattle, Washington, chap 22
- Gomi H, Kawato M (1993) Neural network control for a closed loop system using feed-back-error-learning. *Neural Networks* 6: 933–946
- Gordon AM, Huxley AF, Julian FJ (1966) The variation in isometric tension with sarcomere length in vertebrate muscle fibers. *J Physiol (Lond)* 184:143–169
- Hannaford B, Winters JM (1990) Actuator properties and movement control: biological and technological models. In: Winters J, Woo S (eds) *Multiple muscle systems*. Springer, Berlin Heidelberg New York
- Hannaford B, Winters JM, Chou C-P, Marbot PH (1995) The anthropomorphic arm: a system for the study of spinal circuits. *Ann Biomed Eng* 23:399–408
- Hebb DO (1949) *The organization of behavior: a neuropsychological theory*, Wiley, New York
- Hill AV (1938) The heat of shortening and dynamic constraints of muscle. *Proc R Soc Lond B Biol Sci* 126:136–195
- Inoue K (1988) *Rubbertuators and applications for robots*. Robotics research: the fourth international symposium. MIT Press, Cambridge, Mass
- Lacquaniti F, Licata F, Soechting JF (1982) The mechanical behavior of the human forearm in response to transient perturbations. *Biol Cybern* 44:35–46
- Lan N, Crago E (1994) Optimal control of antagonistic muscle stiffness during voluntary movements. *Biol Cybern* 71:123–135
- Loeb G (1987) Hard lessons in motor control from the mammalian spinal cord. *Trends Neurosci* 10:108–113
- Marbot PH, Hannaford B (1993) The mechanical spindle: a replica of the mammalian muscle spindle. *Proc IEEE Conf Eng Med Biol, San Diego, Calif*
- Marbot PH (1995) Ia response of a mechanical spindle replica. PhD dissertation, University of Washington, Department of Electrical Engineering
- Raibert MH (1978) A model for sensorimotor control and learning. *Biol Cybern* 29:29–36
- Ramos CF, Hacısalihzade SS, Stark LW (1990) Behaviour space of a stretch reflex model and its implications for the neural control of voluntary movement. *Med Biol Eng Comput* 28:15–23
- Schulte HF Jr (1961) The characteristics of the McKibben artificial muscle. In: *The application of external power in prosthetics and orthotics*. National Academy of Sciences, National Research Council, Washington, DC
- Shoemaker M (1993) A study and model of the role of the Renshaw cell in regulating the transient firing rate of the motoneuron. MSEE thesis, University of Washington, Department of Electrical Engineering, June 1993
- Shoemaker M, Hannaford B (1994) A study and model of the role of the Renshaw cell in regulating the transient firing rate of the motoneuron. *Biol Cybern* 71:251–262
- Snell RS (1980) *Clinical anatomy for medical students*, 2nd edn. Little, Brown, Boston
- Zuckerman JD, Matsen FA III (1989) Biomechanics of the elbow. In: Frankel VH (ed) *Basic biomechanics of the musculoskeletal system*. Lea & Febiger, Philadelphia, chap 13